

Image guidance in deep brain stimulation surgery to treat Parkinson's disease: a review

Yiming Xiao, *Member, IEEE*, Jonathan C. Lau, Dimuthu Hemachandra, Greydon Gilmore, Ali R. Khan, *Member, IEEE*, and Terry M. Peters, *Life Fellow, IEEE*

Abstract—Deep brain stimulation (DBS) is an effective therapy as an alternative to pharmaceutical treatments for Parkinson's disease (PD). Aside from factors such as instrumentation, treatment plans, and surgical protocols, the success of the procedure depends heavily on the accurate placement of the electrode within the optimal therapeutic targets while avoiding vital structures that can cause surgical complications and adverse neurologic effects. While specific surgical techniques for DBS can vary, interventional guidance with medical imaging has greatly contributed to the development, outcomes, and safety of the procedure. With rapid development in novel imaging techniques, computational methods, and surgical navigation software, as well as growing insights into the disease and mechanism of action of DBS, modern image guidance is expected to further enhance the capacity and efficacy of the procedure in treating PD. This article surveys the state-of-the-art techniques in image-guided DBS surgery to treat PD, and discusses their benefits and drawbacks, as well as future directions on the topic.

Index Terms—Deep brain stimulation, surgical navigation, neurosurgery, Parkinson's disease, image processing, MRI

**This work has been submitted to the IEEE for possible publication. Copyright may be transferred without notice, after which this version may no longer be accessible.*

I. INTRODUCTION

AFFECTING more than 10 million people worldwide, Parkinson's disease (PD) is a chronic and progressive neurodegenerative disorder. Although it is still primarily characterized by related motor symptoms, including tremor, muscle rigidity and bradykinesia, the associated non-motor symptoms are being increasingly recognized. In addition to pharmacotherapy, deep brain stimulation (DBS) is a surgical treatment that can improve dopamine-related motor dysfunctions of the disorder, by implanting electrodes to

stimulate designated regions in the brain. Often, intra-operative micro-electrode recording (MER) is performed to confirm or refine the therapeutic target determined in the pre-surgical plan before the DBS lead is placed and secured in place. With the more commonly employed stimulation targets of the subthalamic nucleus (STN) and globus pallidus interna (Gpi) to treat PD, the ventral intermediate nucleus (Vim) of the thalamus is an option for tremor-dominated PD.

In DBS surgery, the electrode must be inserted through a bur-hole to reach the optimal locus without damaging vital anatomy (e.g., blood vessels and ventricles) or stimulating other brain structures that can induce adverse responses [1]. The procedure has three main challenges. First, the DBS targets are often relatively small and poorly visualized using conventional medical imaging techniques for neurosurgical planning. Second, to avoid complications and unwanted outcomes, DBS lead insertion planning needs to consider various medical images that reveal different physiological information, which can be challenging and time-consuming for the surgeon to navigate. Finally, intra-operative tissue shift and post-operative DBS lead migration can occur, and intra-operative refinement of stimulation target is often needed. Since the inception of DBS, image guidance has played important roles to tackle these issues from three major directions, including surgical targeting, navigation, and monitoring. In targeting, many specialized MRI techniques and computational methods have been developed to reveal the location and geometry of the surgical targets, especially for the STN, and more recently, to ensure optimal functional outcomes via incorporating functional and neural connectivity data. In general, based on the approaches used, the targeting methods can be grouped into structural and functional categories. The structural category can be further organized into indirect and direct methods. For surgical navigation, multiple neuronavigation software packages, with graphical rendering of surgical data, feature integrated image-processing algorithms, and automatic lead trajectory planning have been proposed to facilitate both pre-surgical planning and post-hoc outcome analysis. Lastly, for DBS monitoring, imaging and computational methods have been pursued to ensure correct electrode placement, as well as potentially monitoring functional responses to the stimulation and hemorrhage.

Image-guidance in DBS surgery is a highly multi-faceted topic that involves image acquisition, image processing, computational models, and physiological modeling of the tissue and brain function. The advancement of DBS image guidance is imperative to ensure and possibly extend the DBS outcomes. while simultaneously offering needed insights

Manuscript received xxxx.

Y. Xiao, J.C. Lau, D. Hemachandra, A.R. Khan, and T. M. Peters are with Robarts Research Institute, Western University, London, N6A 5B7, Canada (e-mail: yxiao286@uwo.ca).

J.C. Lau is with the Department of Clinical Neurological Sciences, Division of Neurosurgery, Western University, London, Canada

D. Hemachandra, G. Gilmore, A.R. Khan, and T. M. Peters are with the School of Biomedical Engineering, Western University, London Canada.

A.R. Khan, and T. M. Peters are with the Department of Medical Biophysics, Schulich School of Medicine and Dentistry, Western University, London, Canada.

A.R. Khan is with the Brain and Mind Institute, Western University, London, Canada.

regarding our brain circuitry and the true potential of DBS, as well as providing the knowledge for other therapies (e.g., focused-ultrasound surgery). This review primarily focuses on current methodological developments of image guidance for DBS to treat PD, in the three aforementioned aspects. Since more existing methods are devoted to surgical targeting, the review of this aspect is proportionally longer than the other two. A schematic of this review is shown in Fig. 1.

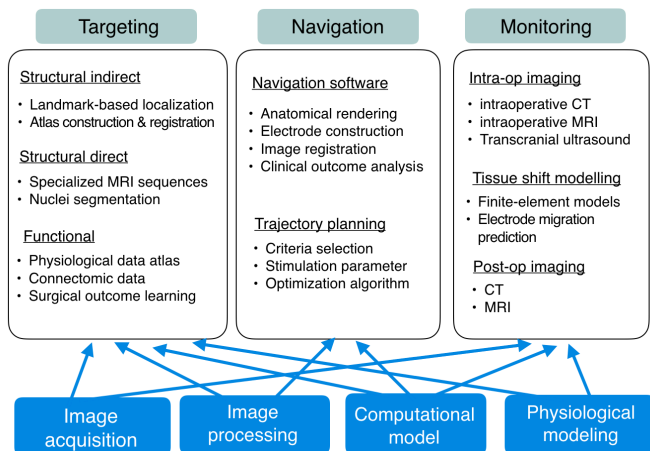


Figure 1. Schematic of different components reviewed in image-guidance for DBS surgery to treat Parkinson's disease.

II. STRUCTURAL INDIRECT TARGETING

Indirect targeting approaches infer the centroid or geometry of the nucleus either from adjacent anatomical features, or by fitting an atlas to an individual's anatomy as represented in pre-operative scans (e.g., T1w MRI) that fail to sufficiently visualize the target. This approach was used historically before the era of modern imaging, and to this day is still often used as a first approximation of the target location.

A. Coordinate-based approaches

Conventionally, the locations of the surgical targets are often inferred from their spatial coordinates in relation to more easily identifiable anatomical landmarks, as defined in well-established atlases such as those from Talairach [2] or Schaltenbrand atlases [3]. Among different coordinate systems, the mid-point (i.e., middle commissure or MC) between the line connecting anterior commissure (AC) and posterior commissure (PC) (see Fig.2) is the most popular landmark to help locate the surgical targets, such as the STN. Efforts were therefore, made to improve the accuracy, consistency, and automation of AC and PC identification [4, 5] through multi-template registration and local image feature learning as well as developing open standards for placing these features [6]. To adjust for individual variability, the coordinates are usually scaled by a factor that normalizes AC-PC line lengths between the patient's anatomy and the atlas employed, and some also use additional adjustments based on considerations, such as the third ventricle width [7], but there remains a lack of consensus among the specialists [8].

B. Structural brain atlases and image registration

Distinct from coordinate-based targeting that only offers points in 3D, full geometry and richer anatomical context can be obtained for the surgical target, by mapping structural brain atlases to the patient's anatomy, using volume-to-volume image alignment. Besides the more recent digitized Talairach [2] or Schaltenbrand atlases [3], a number of brain atlases have been released to benefit DBS planning. As a starter, several subcortical atlases have been developed from 3D reconstruction of histological annotations [9-11], and were co-registered to single-subject T1w MRI templates. For better anatomical representation, atlases averaged from a group of subjects have become a standard practice. In 2013, Haegelen *et al.* [12] built a PD-population-averaged atlas (named ParkMedAtlas) with manual segmentation of 7 pairs of subcortical structures. Xiao *et al.* [13, 14] constructed the MNI PD25 atlas with a novel T1-T2*-fusion contrast template and a co-registered histological atlas with 123 structure labels, and the ultrahigh-resolution BigBrain atlas [15, 16] (Fig.3a). More recently, Inglesias *et al.* [17] published a probabilistic atlas of the human thalamic nuclei with *ex vivo* MRI and histology of 6 elderly subjects, and the new CIT168 atlas (Fig.3b&c) was created from 168 young healthy subjects by Pauli *et al.* [18]. Benefiting from enhanced tissue contrast of ultra-high field 7T MRI, Keuken *et al.* [19] and Wang *et al.* [20] proposed multi-contrast averaged brain atlases with probabilistic maps of the basal ganglia structures using healthy subjects, which was applied prospectively in surgical cases [21]. Besides anatomy, atlases that include functional sub-divisions of target nuclei were also proposed, intended to better pin-point the therapeutic subregion. In this vein, Silva *et al.* [22] and Accolla *et al.* [23] provided parcellation for the GPi and STN, respectively. Based on the atlas of Chakravarty *et al.* [11], the DISTIL atlas [24] sub-divides the STN and GPi into 3 different functional zones in the MNI152 template space.

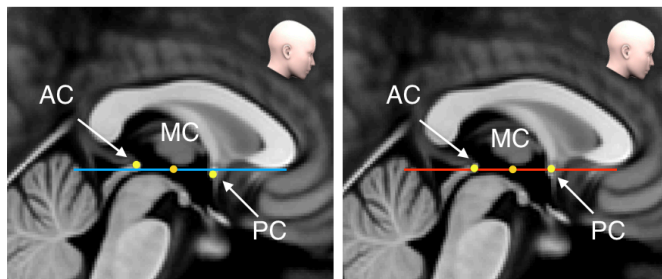


Figure 2. AC-PC lines and MC points defined in Talairach atlas space (Left) and Schaltenbrand atlas space (Right), shown in the mid-sagittal plane of the T1w ICBM152 template. Note that the differences in the definition of AC-PC, and thus the reference coordinates to locate surgical targets.

Atlas-to-MRI registration strategies can impact the quality of targeting. In indirect targeting, such registration relies only on T1w MRI. Bardin *et al.* [25] used the patient's original and mirrored MRI to improve the atlas registration accuracy. Duay *et al.* [26] proposed an active-contour-based atlas registration for STN targeting. Using the Colin27 template [27] as a medium, Chakravarty *et al.* [28] employed pseudo-MR images

derived from digitized histological atlases to map the atlas to individual patients. Finally, different deformation models and publicly available registration software were assessed by Chakravarty *et al.* [29] and Ewert *et al.* [30], confirming the need for refined nonlinear warping.

III. STRUCTURAL DIRECT TARGETING

Direct targeting locates the surgical targets using MRI techniques and the associated image processing methods that can directly visualize them. Among these, 2D fast spin-echo (FSE) T2w MRI has the longest history in the clinic. However, such images are slow to acquire, making it difficult for the patients to tolerate. Often highly anisotropic resolution (3~5 mm axial slice thickness) images, or just a slab of the brain is obtained. Newer MRI sequences primarily aim to enhance the contrast of the nuclei, image quality (e.g., signal-to-noise ratio and image resolution), or scanning efficiency. Full summaries of MRI sequences and nuclei segmentations are included in *Tables S1 & S2* of the supplementary material.

A. Inversion recovery imaging

Inversion recovery (IR) imaging that reduces signals from designated tissues can boost the contrasts of subcortical structures. Ishimori *et al.* [31] proposed a 3D phase sensitive IR sequence with image contrast optimization to visualize the STN. Sudhyadhom *et al.* [32] proposed the Fast Gray matter Acquisition T1 Inversion Recovery (FGATIR) image to highlight the boundaries of subcortical structures and improve atlas fitting, demonstrating that FGATIR is superior to T2-FLAIR in providing contrast between nuclei. Kitajima *et al.* [33] compared the FSE T2w and fast short inversion time IR (FSTIR) images, and concluded that it is easier to differentiate the STN from the adjacent SN in FSTIR images. Later, Nowacki *et al.* [34] evaluated the application of the modified driven equilibrium Fourier transform (MDEFT) sequence for depicting the GPi, though it was shown that magnetization transfer (MT) maps can better visualize the GP than MDEFT [35].

B. Susceptibility-weighted imaging

Susceptibility-weighted imaging (SWI) enhances the contrast of the subcortical structures by taking advantage of their rich iron deposition. A typical SWI sequence produces a T2*w MRI, a phase image, and a magnitude-phase-fusion contrast. While the magnitude-phase-fusion image was originally intended for venography, the sequence has subsequently been customized to visualize the STN for DBS. Vertinsky *et al.* [36] optimized the scanning parameters of single-echo SWI images to best visualize the STN, and reported that the phase image is the best for the purpose. T2*w MRI exhibit high contrast for subcortical structures, but also exhibits evident susceptibility artifacts, which requires additional T1w MRI in surgical planning and may affect image registration quality. Xiao *et al.* [37] proposed a 10-echo FLASH sequence that produces different contrasts, including T1w and T2*w MRIs, whose image quality was enhanced through averaging adjacent echoes and optimizing scanning parameters. Alternatively, Volz *et al.* [38] attempted to recover the signal loss from susceptibility artifacts, by estimating pixel-wise signal loss

and adaptively fusing multi-echo data. Finally, Wu *et al.* [39] proposed an inverse double-echo steady-state (iDESS) technique to depict the midbrain nuclei and reduce susceptibility signal loss.

C. Quantitative imaging

Quantitative MRI techniques can reveal the microstructural architectures of brain tissues by deriving their intrinsic MRI properties, including T1, T2, T2*, susceptibility, and magnetization transfer (MT) parameters. Therefore, these quantitative maps offer the opportunity to better describe the boundary between adjacent tissue types. Guo *et al.* [40] introduced the driven equilibrium single pulse observation of T1 and T2 (DESPOT1 and DESPOT2 [41], respectively) for DBS implantation. Helms *et al.* [35] proposed a novel, semi-quantitative magnetization transfer (MT) imaging to improve contrast of basal ganglia structures, and discussed its feasibility in anatomical localization for DBS. Aside from the standard contrasts from the SWI sequence, T2* or R2* (1/T2*) maps [42] and later quantitative susceptibility maps (QSMs) [43] can also be derived to help improve the visualization of the STN and GP.

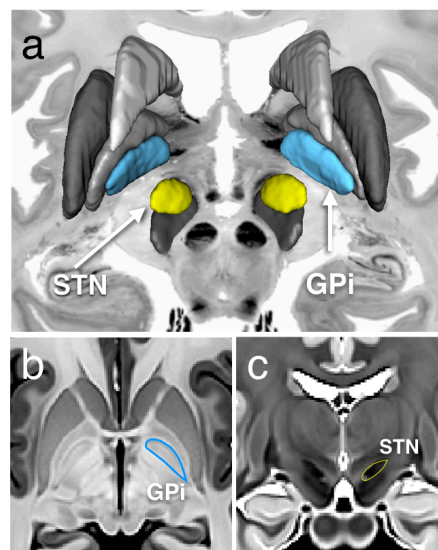


Figure 3. (a) The STN and GPi rendered in 3D with other basal ganglia structures in the histological BigBrain atlas [15, 16]; (b) GPi is shown in axial view of the T1w CIT168 atlas [18]; (c) STN is shown in the coronal view of the T2w CIT168 atlas.

D. Ultra-high field MR imaging

Ultra-high field (>3T) MRI can boost the sensitivity, resolution, and signal-to-noise ratio of functional and anatomical images, and thus can offer more exquisite anatomical details. Abosch *et al.* [44] obtained T2w and SWI scans at 7T, and showcased the superior ability to effectively improve the identification of the GPi, STN, and Vim. Duchin *et al.* [45] found that T2w MRI at 7T has minimal distortion within the central part of the brain compared with at 1.5T, and thus is suitable for clinical use. Cho *et al.* [46] compared T2*w MRI at 1.5, 3, and 7T for visualizing the STN, while Deistung *et al.* [43] compared the contrast of subcortical structures in QSM, T2*w, phase, and R2* images at 7T, and

concluded that QSM demonstrates the highest anatomical detail.

E. Deep brain nuclei segmentation

These aforementioned MRI techniques provide the opportunity for automatic nucleus segmentation to facilitate computer-assisted DBS planning and pathological studies of PD. Thus far, a number of groups have proposed and validated their methods, which can be categorized into atlas-based (single-atlas propagation and multi-atlas label fusion), model-based, and deep learning-based methods. Distinct from atlas-based segmentation in indirect targeting, the methods in this section involve image contrasts that display the nuclei of interest with sufficient contrast for registration or atlas selection. With a larger volume and visibility in T1w MRIs, segmentation of the GPi is more commonly reported. As for STN segmentation, Haegelen *et al.* [12] compared methods including single atlas propagation with different registration algorithms, ANIMAL [47] and SyN [48], and a non-local means label-fusion method [49] to segment subcortical regions using high-resolution sectional T2w FSE MRI at 3T. Their comparison offered the best results with a 0.64 Dice score using the ANIMAL algorithm. Also with 3T data, Xiao *et al.* [50] employed T2w pseudo-MRI to improve histological atlas registration to segment the STN. Later, to resolve the drawbacks of single-atlas propagation [51], the same group proposed label fusion segmentation methods for the midbrain nuclei, using fuzzy majority-voting on T2w MRI [51] and multi-contrast non-local means on SWI data [52], with the Dice score ranging 0.74–0.90 for their approaches. With respect to model-based approaches, Li *et al.* [53] used a band-limited level set to segment the STN on 3T T2w MRI. At 7T, Visser *et al.* [54] used both shape and multi-spectral intensity (QSM, T2w, T2*w, and fractional anisotropy map) modeling to segment the midbrain nuclei, while Kim *et al.* [55] used regression models to identify the STN in 1.5T T2w MRI based on a 7T training set. Most recently, deep learning has been employed to identify the STN [56], achieving a Dice coefficient of 0.90. Intending to serve a wider community, Manjon *et al.* [57] proposed *pBrain*, an online processing pipeline for segmenting the STN based on multi-atlas label-fusion with multiple -scales and features in T2w MRI.

IV. TARGETING WITH FUNCTIONAL DATA

Distinct from the previous two categories that focus on providing the centroid or geometry for the anatomy to be stimulated, targeting with functional data is centered around the concept that targeting a specific functional region within the nucleus of interest may provide the maximum symptom improvements while minimizing adverse effects. Three general categories of functional targeting have been reported: probabilistic functional atlas mapping; connectivity-based targeting; and machine learning for surgical outcome. A summary of all currently available methods is available in *Table S3* in the supplementary material.

Among the various approaches, the probabilistic functional atlas mapping has the longest history. For this type of atlas, the locations of the active electrodes, the responses to

stimulation, and the stimulator settings, are recorded for each individual patient. The stimulation locations of a cohort of patients with sufficient clinical benefits were deformed to a common anatomical atlas, while the influence of the applied electric field was modeled by a kernel function. Finally, the results were averaged to form a probabilistic representation of the “hot spot” to guide loci selection. As the earliest to develop such atlases, Nowinski *et al.* [58, 59] showed that DBS planning with their probabilistic functional atlas is better than solely relying on an anatomical atlases. Guo *et al.* [60] also presented a probabilistic atlas, built from intra-operative data of Finnis *et al.* [61], and demonstrated the advantage of the functional atlas in comparison to other anatomy-based approaches [40]. To further improve atlas-to-patient registration for stimulation target selection, D’Haese *et al.* [62, 63] proposed a multi-template technique for their electrophysiological atlas, and reported < 1.75mm mean deviation from final implanted location when using the atlas for planning. From the same group, Pallavaram *et al.* [64] used spherical kernels instead of more commonly seen Gaussian kernels [60] to more accurately reflect the effect of electric stimulation.

The second category of techniques utilize brain connectivity data, derived from diffusion and functional MRI to locate therapeutic neural pathways and sub-regions of nuclei that are difficult to visualize in structural MRI. Tractography obtained from diffusion MRI has been employed to determine optimal electrode placement within sub-regions of the STN [65, 66] and GPi [67]. Since the Vim nucleus of the thalamus is difficult to visualize on structural images, both tractography [68] and task-based functional MRI [69] have been used to help locate it. More specifically, Sammartino *et al.* [68] reported a mean discrepancy of 1.6mm between targeting using tractography and actual surgical choice. The extraction of dentatorubrothalamic (DRT) tract using tractography by obtaining tracts passing the dentate nucleus, thalamus, and motor cortex has been proposed as an alternative image-based target for tremor [70]. Compared with the first category of functional targeting that relies on the collection of previous target locations, connectivity-based targeting, often referred to as connectomic DBS, links the therapeutic benefits with activation of specific neural pathways.

Lastly, the new data-driven approaches rely on machine learning to predict surgical outcomes at intended stimulation locations. Horn *et al.* [71] used brain connectivity data and linear regression models to calculate the surgical outcomes with an average 15% error margin for Unified Parkinson’s Disease Rating Scale (UPDRS) motor score improvements. Later, Baumgarten *et al.* [72] trained an artificial neural network model with 3D coordinates and levels of electric current to predict whether selected stimulation loci induce therapeutic benefits and side effects, obtaining the sensitivity of 93.07% and 73.47%, respectively. Similarly, Lin *et al.* [73] newly proposed a random forest classifier to differentiate ineffective vs. effective targets, but using instead a mean fractional anisotropy and tractography streamline fraction of the stimulation site within the STN to the rest of the brain. Their approach achieved a classification accuracy of 84.9%.

V. DBS NAVIGATION SOFTWARE & TRAJECTORY PLANNING

Surgical navigation software provides the needed interface to visualize complex clinical information, pre-process imaging data, and possibly devise surgical plans, as well as perform post-hoc outcome analysis. Aside from commercial software, a number of DBS navigation software platforms have been developed for research purposes. The summary of the various current research-based navigation systems is listed in *Table S4* of the supplementary material.

As the first of its kind, CranialVault [74] packaged automatic image processing tools, data visualization, and functional target selection [18] into one user interface. PyDBS [75] and IBIS NeuroNav [76] also offer surgical data visualization for planning DBS. With the first containing streamlined workflow to segment and register multi-modal scans, both of them incorporate efficient and automatic trajectory planning tools [77-80] as software plug-in extensions. Primarily to help analyze post-surgical impacts, PaCER [81] and DBSproc [82] were built to more accurately reconstruct the electrodes and offer tractographic analysis of surgical targets. On the similar note, LeadDBS [83] provides a platform to conduct statistical analysis for DBS procedures with integrated registration tools, an electrode reconstruction function, and integrated brain atlases, including both structural and connectomic types.

A safe trajectory for DBS electrode insertion should consider multiple criteria, including but not limited to the distance to the optimal stimulation target while avoiding cerebral vasculature, ventricles, and structures, such as posterior limb of the internal capsule, that can induce adverse effects. However, proposing viable insertion paths by simultaneously considering all these conditions may impose a heavy cognitive demand for the surgeon, making the process arduous and time-consuming. Therefore, several automated trajectory planning algorithms have been proposed by framing the task as optimizing cost functions that represent these criteria mathematically.

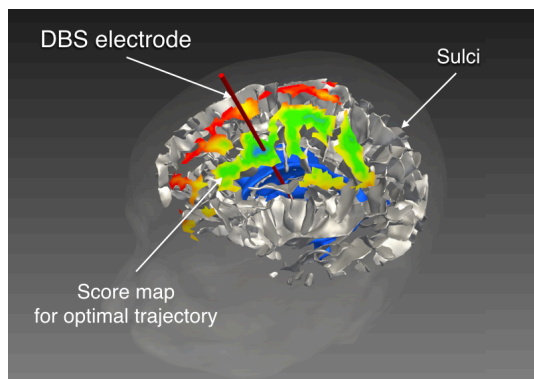


Figure 3. Demonstration of the automatic DBS trajectory planning software proposed by Essert *et al.* [79, 80] in a case of STN stimulation (Courtesy of Dr. Caroline Essert, University of Strasbourg)

While the earlier versions [84, 85] of these algorithms demonstrated the feasibility of such optimization frameworks with limited criteria, more recent approaches [77-80]

incorporated a larger set of constraints, as well as introduced new data types into the optimization procedure. From the Montreal Neurological Institute group, Bériault *et al.* [77, 78] proposed automated DBS planning using SWI venography to ensure surgical safety and introduced a computational model for STN DBS stimulation with multiple active electrode contacts. In a similar vein, Essert *et al.* [80] emphasized the geometry of the insertion paths in their algorithm, and assessed the performance retrospectively. Later, Dergchyova *et al.* [79] further developed the Essert system, allowing the cost function to balance both the functional improvement predicted by probabilistic efficacy maps and the surgical risks. Despite various successes in automated trajectory planning algorithms, the strategy to weigh various path planning criteria is still largely determined by the users in a trial-and-error manner, and no systematic studies have been conducted to provide a unified framework to determine the optimal weights.

VI. INTRA-OPERATIVE AND POST-OPERATIVE MONITORING

Intra-operative monitoring can ensure the safety and quality of DBS, and the technical advancements have made it feasible to inspect many crucial factors during surgery, including electrode position, brain shift, intra-operative hemorrhage, and functional responses to stimulation. This is especially helpful for brain shift in DBS, which is able to impact surgical quality [86-88] in both intra-operative targeting and post-surgical electrode migration, with an averaged electrode shift of 1.41 mm measured by Sillay *et al.* [86]. So far, besides more conventional and costly intra-operative MRI (iMRI) [89] and intra-operative CT (iCT) systems, transcranial sonography (TCS) [90, 91] and bio-mechanical modeling [87, 92] have also been reported. iCT is typically used to confirm the electrode position, and while it is an accurate equivalent to post-operative MRI measurement [88], it lacks soft tissue contrast. Besides electrode position verification, iMRI [89] can provide different image contrasts that visualize the surgical target, brain shift, and hemorrhage, and perform intra-operative fMRI [93] to possibly refine electrode placement and stimulation parameters. A more cost effective modality, 3D TCS was tested experimentally to guide DBS electrode placement [91]. With a limited accuracy of electrode tip localization [90] due to challenges in TCS-MRI fusion and image distortion, the method is not yet ready for clinical use. Lastly, finite element models (FEMs) [87, 92] have also been demonstrated in simulation [87] and clinical case study [92] to improve the electrode placement by accounting for brain shift, but further developments that allow efficient integration into the clinical workflow are needed.

Post-operative imaging is another crucial step to verify final electrode position, particularly for potential electrode migration, assessment of surgical complications, and investigation of physiological impacts of the treatment. Recent studies [94, 95] with post-operative structural and functional MRI, have revealed the tissue and functional changes after DBS surgery. While CT avoids the need for meticulous estimation of heat dissipation with MRI in the presence of a DBS electrode, the physiological insights offered is limited. Studies [96] have recommended a specific absorption rate

(SAR) below 0.1 W/kg when planning post-operative MRI for DBS cases.

VII. DISCUSSION

A. Targeting: coordinates, anatomy, and function

Atlas coordinate-based DBS targeting has a long history in the clinic. It assumes that the relative positions and sizes of DBS surgical targets, such as the STN, are consistent across subjects, and can tolerate minimum or lower quality imaging data. Meanwhile, non-negligible anatomical variability across subjects [51, 97, 98] has also been reported for the surgical target. The choice between the coordinate-based technique and direct targeting has been actively debated, largely for localizing the STN. While the earlier reports favored the first [99], more recent evidence [51, 98] prefer the latter. This discrepancy may likely be attributed to the improved image quality of MRI scanners, especially in terms of signal-to-noise ratio, image resolution, and newer scanning sequences, but unfortunately most studies [99] only reported results with fairly limited patients, or even healthy cohorts. Notably, the initial stimulation locations derived from coordinate-based methods and anatomical MRI are usually the estimated centroid or geometric center of the nucleus, which is often different from the therapeutic target. Inputs from functional information at the planning stage can therefore be important. Such insights can be made available through brain atlases that contain connectivity-based sub-divisions of the nucleus [24], probabilistic representation of effective stimulation loci [60, 64], and group-averaged connectomes [71]. With physiological recording [100], we have observed that therapeutic regions are not necessarily bounded by the borders of a particular anatomy. To push this notion further, functional targeting with brain connectivity data, including diffusion and functional MRI, allows effective and tailored stimulation of nuclei subregions [101] or instead towards white matter pathways [70, 102] for targeted symptoms.

Both indirect and direct targeting methods, and even many functional targeting approaches, have relied heavily on brain atlases, where significant progress has been made in adding super-high-resolution histological data [16], multi-contrast MRI [9, 13, 20, 64, 97], unbiased anatomical representation, and brain connectivity information [67, 71]. To accurately transfer the rich information from the atlases to an individual's anatomy, suitable registration strategies are crucial. As anatomical variability in midbrain nuclei was revealed by high-quality structural MRI [51, 97], refined non-linear registration strategies [29, 30] are needed, and multi-contrast registration [16, 50, 71] is recommended for targets that are not visible on T1w MRI. Aside from brain atlas customization, concerns [103] have also been raised regarding potential insufficient representation of individual physiology when using group-averaged connectomic atlases for DBS planning. Comprehensive investigation is still required to confirm the impact of these approaches.

Selecting the appropriate ground truth to assess DBS targeting methods is crucial and challenging. Typical references [99] to validate DBS planning techniques include final implantation

locations shown in post-operative scans, intra-operative recording locations, coordinates shown in established atlases, structural MRI, and post-surgical symptom improvement. With possible tissue shift and electrode migration, stimulation targets determined during and after surgery may not overlap, and they may also exhibit an inherent bias away from the pre-surgical plans. Although symptom improvement appears more meaningful as a ground truth, the possibility of alternative candidate targets with better outcomes make it difficult to assess prospective cases. Surprisingly, some functional targeting approaches [59, 69] used atlas coordinates as ground truth, which is not ideal, and the differences in validation metrics make it difficult to conduct cross-method comparisons. Finally, most reported planning techniques focus only on single contact stimulation. Multi-contact DBS planning, which is more complex to validate, is seldom mentioned in the literature.

B. MR imaging and segmentation of surgical targets

To date, a majority of the literature on novel structural MRI sequences for DBS is dedicated to the STN, for which, susceptibility-based contrasts [36, 37, 42, 44, 46], particularly 7T QSM [43] showed superior results. Most MRI techniques surveyed in *Table S1* were only developed based on small cohorts with primarily healthy subjects. This may affect their performance in PD patients, who can exhibit varied biochemical features in the brain and are less tolerant to relatively long scan sessions. In these novel sequences, typical slice thickness is still 2 mm, which is not ideal to accurately depict the geometry of the small STN, and is also in contrast to the finer isotropic resolutions used in automatic segmentations in *Table S2*. Unfortunately, none of these newer sequences has been reported in routine surgical practice in the literature. Another important factor of MR imaging for DBS is geometric distortion, which can originate from various sources, such as magnetic field inhomogeneity, chemical shift, and susceptibility differences. This factor was only assessed by Ishmori *et al.* [31] and Duchin *et al.* [45] in their studies, without disentangling individual contributing sources. With ultra-high field 7T MRI becoming more available, the inherent issues of image distortion from increasing field strength, particularly magnetic field inhomogeneity, will require rigorous examination [104].

Automatic segmentation algorithms for the STN have provided excellent results, achieving a Dice score of nearly 0.90. Unlike other brain structures that can be easily visualized in standard T1w MRI, the technical developments for segmenting DBS targets, especially deep learning algorithms, were encumbered by limited quality MRI databases, the lack of the unified segmentation protocols, and effective MRI technique development. Yet, the existing techniques may not offer the same accuracy as reported on clinical scans, which often exhibit poorer rougher image quality.

Although the benefits of connectomic DBS surgery are becoming increasingly evident, especially for targets that are difficult to depict solely by structural imaging, high quality diffusion and functional MRI face challenges in their integration into clinical routines. This makes development and

validation of relevant functional targeting algorithms with large clinical databases more challenging.

C. Intra-operative and post-operative imaging in DBS

Surgical target shift in DBS due to intraoperative tissue shift has been measured to be more than 2mm in some cases [92, 105, 106]. However, aside from surgical protocols that avoid CSF leakage to reduce this phenomenon, no effective algorithms similar to those in brain tumor resection [107] have been proposed based on inter-operative imaging for tissue shift correction. Intra-operative fMRI [93] offers the possibility of real-time monitoring for the impacts of DBS to improve the final targeting, but the high cost and special requirements for surgical setup make it difficult to access. Aside from confirming electrode position, post-operative MRI can also play a valuable role in advancing our understanding of the mechanism and true impacts of DBS [94, 95]. For both intra-operative and post-operative imaging, image artifacts (e.g., streaking and distortion) induced from DBS leads can pose difficulty in obtaining accurate knowledge of final implantation location, and need to be carefully considered in imaging and outcome analysis.

D. Future directions

Studies [108] have indicated that instead of local circuitry modulation, DBS may exhibit widespread effects on the brain. Although still at the early stage, preliminary retrospective studies in connectomic DBS [70, 71, 73] have shown great potentials. The surgical strategy may eliminate or at least minimize the need for MER, potentially resulting in shorter operation time and improved patient comfort. The use of brain connectivity information in DBS planning and analysis will continue to enrich our understanding of the neural circuitry and the mechanism of DBS in the future.

Current DBS strategy focuses primarily on dopamine-related motor symptoms of PD, and the non-motor issues (e.g., psychiatric symptoms and cognitive declines) are rarely considered. In addition, traditional stimulation targets, such as STN and GPi still have their limitations in therapeutic benefits and side effects [109]. These motivate the search for new DBS targets to treat PD, and a number of potential candidates, including individual nuclei and fiber pathways, have been proposed [70, 110], as well as multi-target stimulation to boost the impacts [111]. These demands pose two challenges on image-guidance of DBS. First, continued efforts are still needed to develop new MRI (structural and functional) techniques and the associated analysis methods to help identify the structures/pathways and confirm their impacts. Second, with richer image modalities required to improve DBS strategy, the challenges of multi-target stimulation, and new DBS devices, DBS navigation software will need to provide more intuitive and resource-efficient strategies for data visualization [112] and updated algorithms for improved electrode trajectory planning.

Machine learning and deep learning techniques have shown early success in facilitating DBS planning in anatomical segmentation [53, 55-57], stimulation target selection [72, 73], and treatment outcome prediction [71]. While these techniques

will continue to develop in the future to benefit the clinic, most of them have relied on limited research-grade MRI scans, whose resolution and image quality are superior to clinical images. Recent developments in deep-learning-based fast MRI [113], image denoising [114], and super resolution [115], along with hardware improvements, are expected to facilitate improved clinical data acquisition. Together with the open data initiatives that enable growing publicly available imaging repositories, learning-based methods may play a more important role in the future.

The development of image-guidance techniques can also benefit other treatments for PD, such as focused ultrasound (FUS) [116]. In addition, it can also greatly contribute to asleep DBS surgery [117], where the electrode is implanted under general anesthesia, to improve the patient's comfort.

VIII. CONCLUSION

This review provides the state of the art for medical image guidance in targeting, navigation, and monitoring of the DBS procedure to treat Parkinson's disease. With an increasing demand for more enhanced and personalized treatments, future developments in DBS image guidance are expected to focus on incorporating connectomic data for improved functional targeting, updating imaging and neuronavigation techniques for new brain stimulation strategies (e.g., novel targets and multi-target stimulation), and finally, leveraging machine/deep learning to allow translation of the knowledge and tools developed in research for clinical data and workflows. Historically, image guidance in DBS has closely accompanied the birth and evolution of this procedure, and will continue to contribute to its future development by providing in-depth insights of its mechanism and possibly extending its clinical benefits.

ACKNOWLEDGMENT

The work is supported by the BrainsCAN and CIHR fellowships for Y. Xiao. Support from CIHR Foundation grant FDN 201409 is also acknowledged. JC Lau is funded through the Western University Clinical Investigator Program accredited by the Royal College of Physicians and Surgeons of Canada and a CIHR Frederick Banting and Charles Best Canada Graduate Doctoral Award Scholarship.

REFERENCES

- [1] P. A. Starr, "Placement of deep brain stimulators into the subthalamic nucleus or globus pallidus internus: Technical approach," *Stereotactic and Functional Neurosurgery*, vol. 79, pp. 118-145, 2002.
- [2] J. T. Talairach, P., "Co-Planar Stereotaxic Atlas of the Human Brain," ed. New York: Thieme Medical Publishers, 1988.
- [3] W. Schaltenbrand G.; Wahren, *Atlas for stereotaxy of the human brain*, 2nd ed. Chicago: Year Book Medical Publishers, 1977.
- [4] B. A. Ardekani and A. H. Bachman, "Model-based automatic detection of the anterior and posterior commissures on MRI scans," *Neuroimage*, vol. 46, pp. 677-682, Jul 1 2009.
- [5] Y. Liu and B. M. Dawant, "Automatic Detection of the Anterior and Posterior Commissures on MRI Scans using Regression Forests," *2014 36th Annual International Conference of the Ieee Engineering in Medicine and Biology Society (Embc)*, pp. 1505-1508, 2014.
- [6] J. C. Lau, A. G. Parrent, J. Demarco, G. Gupta, J. Kai, O. W. Stanley, et al., "A framework for evaluating correspondence between brain

- images using anatomical fiducials," *Human Brain Mapping*, vol. 40, pp. 4163-4179, 2019.
- [7] L. Houshmand, K. S. Cummings, K. L. Chou, and P. G. Patil, "Evaluating indirect subthalamic nucleus targeting with validated 3-tesla magnetic resonance imaging," *Stereotact Funct Neurosurg*, vol. 92, pp. 337-45, 2014.
- [8] W. Hamel, J. A. Koppen, F. Alesch, A. Antonini, J. A. Barcia, H. Bergman, *et al.*, "Targeting of the Subthalamic Nucleus for Deep Brain Stimulation: A Survey Among Parkinson Disease Specialists," *World Neurosurg*, vol. 99, pp. 41-46, Mar 2017.
- [9] J. Yelnik, E. Bardinet, D. Dormont, G. Malandain, S. Ourselin, D. Tande, *et al.*, "A three-dimensional, histological and deformable atlas of the human basal ganglia. I. Atlas construction based on immunohistochemical and MRI data," *Neuroimage*, vol. 34, pp. 618-38, Jan 15 2007.
- [10] K. Niemann, V. R. Mennicken, D. Jeanmonod, and A. Morel, "The Morel stereotactic atlas of the human thalamus: atlas-to-MR registration of internally consistent canonical model," *Neuroimage*, vol. 12, pp. 601-16, Dec 2000.
- [11] M. M. Chakravarty, G. Bertrand, C. P. Hodge, A. F. Sadikot, and D. L. Collins, "The creation of a brain atlas for image guided neurosurgery using serial histological data," *Neuroimage*, vol. 30, pp. 359-76, Apr 1 2006.
- [12] C. Haegelen, P. Coupe, V. Fonov, N. Guizard, P. Jannin, X. Morandi, *et al.*, "Automated segmentation of basal ganglia and deep brain structures in MRI of Parkinson's disease," *Int J Comput Assist Radiol Surg*, vol. 8, pp. 99-110, Jan 2013.
- [13] Y. Xiao, V. Fonov, S. Beriault, F. Al Subaie, M. M. Chakravarty, A. F. Sadikot, *et al.*, "Multi-contrast unbiased MRI atlas of a Parkinson's disease population," *Int J Comput Assist Radiol Surg*, vol. 10, pp. 329-41, Mar 2015.
- [14] Y. Xiao, V. Fonov, M. M. Chakravarty, S. Beriault, F. Al Subaie, A. Sadikot, *et al.*, "A dataset of multi-contrast population-averaged brain MRI atlases of a Parkinsons disease cohort," *Data Brief*, vol. 12, pp. 370-379, Jun 2017.
- [15] K. Amunts, C. Lepage, L. Borgeat, H. Mohlberg, T. Dickscheid, M. E. Rousseau, *et al.*, "BigBrain: an ultrahigh-resolution 3D human brain model," *Science*, vol. 340, pp. 1472-5, Jun 21 2013.
- [16] Y. Xiao, J. C. Lau, T. Anderson, J. DeKraker, D. L. Collins, T. Peters, *et al.*, "An accurate registration of the BigBrain dataset with the MNI PD25 and ICBM152 atlases," *Sci Data*, vol. 6, p. 210, Oct 17 2019.
- [17] J. E. Iglesias, R. Insausti, G. Lerma-Usabiaga, M. Bocchetta, K. Van Leemput, D. N. Greve, *et al.*, "A probabilistic atlas of the human thalamic nuclei combining ex vivo MRI and histology," *Neuroimage*, vol. 183, pp. 314-326, Aug 17 2018.
- [18] W. M. Pauli, A. N. Nili, and J. M. Tyszka, "A high-resolution probabilistic in vivo atlas of human subcortical brain nuclei," *Sci Data*, vol. 5, p. 180063, Apr 17 2018.
- [19] M. F. Keuken, B., "A probabilistic atlas of the basal ganglia using 7 T MRI," *Data Brief*, vol. 4, p. 4, 2015.
- [20] B. T. Wang, S. Poirier, T. Guo, A. G. Parrent, T. M. Peters, and A. R. Khan, "Generation and evaluation of an ultra-high-field atlas with applications in DBS planning," *Medical Imaging 2016: Image Processing*, vol. 9784, 2016.
- [21] J. C. Lau, K. W. MacDougall, M. F. Arango, T. M. Peters, A. G. Parrent, and A. R. Khan, "Ultra-High Field Template-Assisted Target Selection for Deep Brain Stimulation Surgery," *World Neurosurg*, vol. 103, pp. 531-537, Jul 2017.
- [22] N. M. da Silva, S. A. Ahmadi, S. N. Tafula, J. P. S. Cunha, K. Botzel, C. Vollmar, *et al.*, "A diffusion-based connectivity map of the GPi for optimised stereotactic targeting in DBS," *Neuroimage*, vol. 144, pp. 83-91, Jan 1 2017.
- [23] E. A. Accolla, J. Dukart, G. Helms, N. Weiskopf, F. Kherif, A. Lutti, *et al.*, "Brain Tissue Properties Differentiate Between Motor and Limbic Basal Ganglia Circuits," *Human Brain Mapping*, vol. 35, pp. 5083-5092, Oct 2014.
- [24] S. Ewert, P. Plettig, N. F. Li, M. M. Chakravarty, D. L. Collins, T. M. Herrington, *et al.*, "Toward defining deep brain stimulation targets in MNI space: A subcortical atlas based on multimodal MRI, histology and structural connectivity," *Neuroimage*, vol. 170, pp. 271-282, Apr 15 2018.
- [25] E. Bardinet, M. Bhattarjee, D. Dormont, B. Pidoux, G. Malandain, M. Schupbach, *et al.*, "A three-dimensional histological atlas of the human basal ganglia. II. Atlas deformation strategy and evaluation in deep brain stimulation for Parkinson disease," *J Neurosurg*, vol. 110, pp. 208-19, Feb 2009.
- [26] V. Duay, X. Bresson, J. S. Castro, C. Pollo, M. B. Cuadra, and J. P. Thiran, "An active contour-based atlas registration model applied to automatic subthalamic nucleus targeting on MRI: method and validation," *Med Image Comput Comput Assist Interv*, vol. 11, pp. 980-8, 2008.
- [27] C. J. Holmes, R. Hoge, L. Collins, R. Woods, A. W. Toga, and A. C. Evans, "Enhancement of MR Images Using Registration for Signal Averaging," *Journal of Computer Assisted Tomography*, vol. 22, pp. 324-333, 1998.
- [28] M. M. Chakravarty, A. F. Sadikot, J. Germann, G. Bertrand, and D. L. Collins, "Towards a validation of atlas warping techniques," *Medical Image Analysis*, vol. 12, pp. 713-726, Dec 2008.
- [29] M. M. Chakravarty, A. F. Sadikot, J. Germann, P. Hellier, G. Bertrand, and D. L. Collins, "Comparison of piece-wise linear, linear, and nonlinear atlas-to-patient warping techniques: analysis of the labeling of subcortical nuclei for functional neurosurgical applications," *Hum Brain Mapp*, vol. 30, pp. 3574-95, Nov 2009.
- [30] S. Ewert, A. Horn, F. Finkel, N. Li, A. A. Kuhn, and T. M. Herrington, "Optimization and comparative evaluation of nonlinear deformation algorithms for atlas-based segmentation of DBS target nuclei," *Neuroimage*, vol. 184, pp. 586-598, Sep 26 2018.
- [31] T. Ishimori, S. Nakano, Y. Mori, R. Seo, T. Togami, T. Masada, *et al.*, "Preoperative identification of subthalamic nucleus for deep brain stimulation using three-dimensional phase sensitive inversion recovery technique," *Magn Reson Med Sci*, vol. 6, pp. 225-9, 2007.
- [32] A. Sudhyadhom, I. U. Haq, K. D. Foote, M. S. Okun, and F. J. Bova, "A high resolution and high contrast MRI for differentiation of subcortical structures for DBS targeting: the Fast Gray Matter Acquisition T1 Inversion Recovery (FGATIR)," *Neuroimage*, vol. 47 Suppl 2, pp. T44-52, Aug 2009.
- [33] M. Kitajima, Y. Korogi, S. Kakeda, J. Moriya, N. Ohnari, T. Sato, *et al.*, "Human subthalamic nucleus: evaluation with high-resolution MR imaging at 3.0 T," *Neuroradiology*, vol. 50, pp. 675-681, Aug 2008.
- [34] A. Nowacki, M. Fiechter, J. Fichtner, I. Debove, L. Lachenmayer, M. Schupbach, *et al.*, "Using MDEFT MRI Sequences to Target the GPi in DBS Surgery," *Plos One*, vol. 10, Sep 14 2015.
- [35] G. Helms, B. Draganski, R. Frackowiak, J. Ashburner, and N. Weiskopf, "Improved segmentation of deep brain grey matter structures using magnetization transfer (MT) parameter maps," *Neuroimage*, vol. 47, pp. 194-8, Aug 1 2009.
- [36] A. T. Vertinsky, V. A. Coenen, D. J. Lang, S. Kolind, C. R. Honey, D. Li, *et al.*, "Localization of the Subthalamic Nucleus: Optimization with Susceptibility-Weighted Phase MR Imaging," *American Journal of Neuroradiology*, vol. 30, pp. 1717-1724, Oct 2009.
- [37] Y. Xiao, S. Beriault, G. B. Pike, and D. L. Collins, "Multicontrast multiecho FLASH MRI for targeting the subthalamic nucleus," *Magn Reson Imaging*, vol. 30, pp. 627-40, Jun 2012.
- [38] S. Volz, E. Hattingen, C. Preibisch, T. Gasser, and R. Deichmann, "Reduction of susceptibility-induced signal losses in multi-gradient-echo images: application to improved visualization of the subthalamic nucleus," *Neuroimage*, vol. 45, pp. 1135-43, May 1 2009.
- [39] M. L. Wu, H. C. Chang, T. C. Chao, and N. K. Chen, "Efficient imaging of midbrain nuclei using inverse double-echo steady-state acquisition," *Medical Physics*, vol. 42, pp. 4367-4374, Jul 2015.
- [40] T. Guo, K. W. Finnis, S. C. Deoni, A. G. Parrent, and T. M. Peters, "Comparison of different targeting methods for subthalamic nucleus deep brain stimulation," *Med Image Comput Comput Assist Interv*, vol. 9, pp. 768-75, 2006.
- [41] S. C. Deoni, T. M. Peters, and B. K. Rutt, "High-resolution T1 and T2 mapping of the brain in a clinically acceptable time with DESPOT1 and DESPOT2," *Magn Reson Med*, vol. 53, pp. 237-41, Jan 2005.
- [42] R. L. O'Gorman, K. Shmueli, K. Ashkan, M. Samuel, D. J. Lythgoe, A. Shahidiani, *et al.*, "Optimal MRI methods for direct stereotactic targeting of the subthalamic nucleus and globus pallidus," *Eur Radiol*, vol. 21, pp. 130-6, Jan 2011.
- [43] A. Deistung, A. Schafer, F. Schweser, U. Biedermann, R. Turner, and J. R. Reichenbach, "Toward in vivo histology: a comparison of quantitative susceptibility mapping (QSM) with magnitude-, phase-, and R2*-imaging at ultra-high magnetic field strength," *Neuroimage*, vol. 65, pp. 299-314, Jan 15 2013.
- [44] A. Aboosh, E. Yacoub, K. Ugurbil, and N. Harel, "An Assessment of Current Brain Targets for Deep Brain Stimulation Surgery With

- Susceptibility-Weighted Imaging at 7 Tesla," *Neurosurgery*, vol. 67, pp. 1745-1756, Dec 2010.
- [45] Y. Duchin, A. Aboosh, E. Yacoub, G. Sapiro, and N. Harel, "Feasibility of Using Ultra-High Field (7 T) MRI for Clinical Surgical Targeting," *Plos One*, vol. 7, May 17 2012.
- [46] Z. H. Cho, H. K. Min, S. H. Oh, J. Y. Han, C. W. Park, J. G. Chi, *et al.*, "Direct visualization of deep brain stimulation targets in Parkinson disease with the use of 7-tesla magnetic resonance imaging Clinical article," *Journal of Neurosurgery*, vol. 113, pp. 639-647, Sep 2010.
- [47] D. L. E. Collins, A., "Animal: Validation and applications of nonlinear registration-based segmentation," *International Journal of Pattern Recognition and Artificial Intelligence*, vol. 11, p. 24, 1997.
- [48] B. B. Avants, C. L. Epstein, M. Grossman, and J. C. Gee, "Symmetric diffeomorphic image registration with cross-correlation: evaluating automated labeling of elderly and neurodegenerative brain," *Med Image Anal*, vol. 12, pp. 26-41, Feb 2008.
- [49] P. Coupe, J. V. Manjon, V. Fonov, J. Pruessner, M. Robles, and D. L. Collins, "Patch-based segmentation using expert priors: application to hippocampus and ventricle segmentation," *Neuroimage*, vol. 54, pp. 940-54, Jan 15 2011.
- [50] Y. Xiao, L. Bailey, M. M. Chakravarty, S. Beriault, A. F. Sadikot, G. B. Pike, *et al.*, "Atlas-Based segmentation of the subthalamic nucleus, red nucleus, and substantia nigra for deep brain stimulation by incorporating multiple MRI contrasts," presented at the Proceedings of the Third international conference on Information Processing in Computer-Assisted Interventions, Pisa, Italy, 2012.
- [51] Y. Xiao, P. Jannin, T. D'Albis, N. Guizard, C. Haegelen, F. Lalys, *et al.*, "Investigation of morphometric variability of subthalamic nucleus, red nucleus, and substantia nigra in advanced Parkinson's disease patients using automatic segmentation and PCA-based analysis," *Hum Brain Mapp*, vol. 35, pp. 4330-44, Sep 2014.
- [52] Y. M. Xiao, V. S. Fonov, S. Beriault, I. Gerard, A. F. Sadikot, G. B. Pike, *et al.*, "Patch-based label fusion segmentation of brainstem structures with dual-contrast MRI for Parkinson's disease," *International Journal of Computer Assisted Radiology and Surgery*, vol. 10, pp. 1029-1041, Jul 2015.
- [53] B. Li, C. Q. Jiang, L. M. Li, J. G. Zhang, and D. W. Meng, "Automated Segmentation and Reconstruction of the Subthalamic Nucleus in Parkinson's Disease Patients," *Neuromodulation*, vol. 19, pp. 13-19, Jan 2016.
- [54] E. Visser, M. C. Keuken, B. U. Forstmann, and M. Jenkinson, "Automated segmentation of the substantia nigra, subthalamic nucleus and red nucleus in 7 T data at young and old age," *Neuroimage*, vol. 139, pp. 324-336, Oct 1 2016.
- [55] J. Kim, Y. Duchin, H. Kim, J. Vitek, N. Harel, and G. Sapiro, "Robust Prediction of Clinical Deep Brain Stimulation Target Structures via the Estimation of Influential High-Field MR Atlases," *Medical Image Computing and Computer-Assisted Intervention - Miccai 2015, Pt II*, vol. 9350, pp. 587-594, 2015.
- [56] S. C. Park, J. H. Cha, S. Lee, W. Jang, C. S. Lee, and J. K. Lee, "Deep Learning-Based Deep Brain Stimulation Targeting and Clinical Applications," *Front Neurosci*, vol. 13, p. 1128, 2019.
- [57] J. V. Manjon, A. Berto, J. E. Romero, E. Lanuza, R. Vivo-Hernando, F. Aparici-Robles, *et al.*, "pBrain: A novel pipeline for Parkinson related brain structure segmentation," *Neuroimage Clin*, vol. 25, p. 102184, Jan 15 2020.
- [58] W. L. Nowinski, D. Belov, and A. L. Benabid, "An algorithm for rapid calculation of a probabilistic functional atlas of subcortical structures from electrophysiological data collected during functional neurosurgery procedures," *Neuroimage*, vol. 18, pp. 143-155, Jan 2003.
- [59] W. L. Nowinski, A. Thirunavukarasu, J. M. Liu, and A. L. Benabid, "Correlation between the anatomical and functional human subthalamic nucleus," *Stereotactic and Functional Neurosurgery*, vol. 85, pp. 88-93, 2007.
- [60] T. Guo, K. W. Finnis, A. G. Parrent, and T. M. Peters, "Development and application of functional databases for planning deep-brain neurosurgical procedures," *Medical Image Computing and Computer-Assisted Intervention - Miccai 2005, Pt I*, vol. 3749, pp. 835-842, 2005.
- [61] K. W. Finnis, Y. P. Starreveld, A. G. Parrent, A. F. Sadikot, and T. M. Peters, "Three-dimensional database of subcortical electrophysiology for image-guided stereotactic functional neurosurgery," *IEEE Trans Med Imaging*, vol. 22, pp. 93-104, Jan 2003.
- [62] P. F. D'Haese, E. Cetinkaya, C. Kao, J. M. Fitzpatrick, P. E. Konrad, and B. M. Dawant, "Toward the creation of an electrophysiological atlas for the pre-operative planning and intra-operative guidance of deep brain stimulators (DBS) implantation," *Medical Image Computing and Computer-Assisted Intervention - Miccai 2004, Pt I, Proceedings*, vol. 3216, pp. 729-736, 2004.
- [63] P. F. D'Haese, S. Pallavaram, K. Niermann, J. Spooner, C. Kao, P. E. Konrad, *et al.*, "Automatic selection of DBS target points using multiple electrophysiological atlases," *Medical Image Computing and Computer-Assisted Intervention - Miccai 2005, Pt 2*, vol. 3750, pp. 427-434, 2005.
- [64] S. Pallavaram, P. F. D'Haese, C. Kao, H. Yu, M. Remple, J. Neimat, *et al.*, "A New Method for Creating Electrophysiological Maps for DBS Surgery and Their Application to Surgical Guidance," *Medical Image Computing and Computer-Assisted Intervention - Miccai 2008, Pt I, Proceedings*, vol. 5241, pp. 670-+, 2008.
- [65] H. Akram, S. N. Sotiropoulos, S. Jbabdi, D. Georgiev, P. Mählknecht, J. Hyam, *et al.*, "Subthalamic deep brain stimulation sweet spots and hyperdirect cortical connectivity in Parkinson's disease," *Neuroimage*, vol. 158, pp. 332-345, Sep 2017.
- [66] V. A. Coenen, B. Madler, H. Schiffbauer, H. Urbach, and N. Allert, "Individual Fiber Anatomy of the Subthalamic Region Revealed With Diffusion Tensor Imaging: A Concept to Identify the Deep Brain Stimulation Target for Tremor Suppression," *Neurosurgery*, vol. 68, pp. 1069-1075, Apr 2011.
- [67] E. H. Middlebrooks, I. S. Tuna, S. S. Grewal, L. Almeida, M. G. Heckman, E. R. Lesser, *et al.*, "Segmentation of the Globus Pallidus Internus Using Probabilistic Diffusion Tractography for Deep Brain Stimulation Targeting in Parkinson Disease," *American Journal of Neuroradiology*, vol. 39, pp. 1127-1134, Jun 1 2018.
- [68] F. Sannarino, V. Krishna, N. K. K. King, A. M. Lozano, M. L. Schwartz, Y. X. Huang, *et al.*, "Tractography-Based Ventral Intermediate Nucleus Targeting: Novel Methodology and Intraoperative Validation," *Movement Disorders*, vol. 31, pp. 1217-1225, Aug 2016.
- [69] J. S. Anderson, H. S. Dhatt, M. A. Ferguson, M. Lopez-Larson, L. E. Schrock, P. A. House, *et al.*, "Functional Connectivity Targeting for Deep Brain Stimulation in Essential Tremor," *American Journal of Neuroradiology*, vol. 32, pp. 1963-1968, Nov 2011.
- [70] V. A. Coenen, B. Sajonz, T. Prokop, M. Reiser, T. Piroth, H. Urbach, *et al.*, "The dentato-rubro-thalamic tract as the potential common deep brain stimulation target for tremor of various origin: an observational case series," *Acta Neurochir (Wien)*, Jan 29 2020.
- [71] A. Horn, M. Reich, J. Vorwerk, N. Li, G. Wenzel, Q. Fang, *et al.*, "Connectivity Predicts deep brain stimulation outcome in Parkinson disease," *Ann Neurol*, vol. 82, pp. 67-78, Jul 2017.
- [72] C. Baumgarten, C. Haegelen, Y. L. Zhao, P. Sauleau, and P. Jannin, "Data-Driven Prediction of the Therapeutic Window during Subthalamic Deep Brain Stimulation Surgery," *Stereotactic and Functional Neurosurgery*, vol. 96, pp. 142-150, 2018.
- [73] H. Lin, P. Na, D. Zhang, J. Liu, X. Cai, and W. Li, "Brain connectivity markers for the identification of effective contacts in subthalamic nucleus deep brain stimulation," *Hum Brain Mapp*, Jan 17 2020.
- [74] P. F. D'Haese, S. Pallavaram, R. Li, M. S. Remple, C. Kao, J. S. Neimat, *et al.*, "CranialVault and its CRAVE tools: a clinical computer assistance system for deep brain stimulation (DBS) therapy," *Med Image Anal*, vol. 16, pp. 744-53, Apr 2012.
- [75] T. D'Albis, C. Haegelen, C. Essert, S. Fernandez-Vidal, F. Lalys, and P. Jannin, "PyDBS: an automated image processing workflow for deep brain stimulation surgery," *International Journal of Computer Assisted Radiology and Surgery*, vol. 10, pp. 117-128, Feb 2015.
- [76] S. Drouin, A. Kochanowska, M. Kersten-Oertel, I. J. Gerard, R. Zelmann, D. De Nigris, *et al.*, "IBIS: an OR ready open-source platform for image-guided neurosurgery," *Int J Comput Assist Radiol Surg*, vol. 12, pp. 363-378, Mar 2017.
- [77] S. Beriault, F. Al Subaie, K. Mok, A. F. Sadikot, and G. B. Pike, "Automatic trajectory planning of DBS neurosurgery from multi-modal MRI datasets," *Med Image Comput Comput Assist Interv*, vol. 14, pp. 259-66, 2011.
- [78] S. Beriault, Y. Xiao, L. Bailey, D. L. Collins, A. F. Sadikot, and G. B. Pike, "Towards computer-assisted deep brain stimulation targeting with multiple active contacts," *Med Image Comput Comput Assist Interv*, vol. 15, pp. 487-94, 2012.
- [79] O. Dergachyova, Y. L. Zhao, C. Haegelen, P. Jannin, and C. Essert, "Automatic preoperative planning of DBS electrode placement using anatomical atlases and volume of tissue activated," *International Journal of Computer Assisted Radiology and Surgery*, vol. 13, pp. 1117-1128, Jul 2018.

- [80] C. Essert, C. Haegelen, F. Lalys, A. Abadie, and P. Jannin, "Automatic computation of electrode trajectories for Deep Brain Stimulation: a hybrid symbolic and numerical approach," *Int J Comput Assist Radiol Surg*, vol. 7, pp. 517-32, Jul 2012.
- [81] A. Husch, V. P. M. P. Gemmar, J. Goncalves, and F. Hertel, "PaCER - A fully automated method for electrode trajectory and contact reconstruction in deep brain stimulation," *Neuroimage Clin*, vol. 17, pp. 80-89, 2018.
- [82] P. M. Lauro, N. Vanegas-Aroyave, L. Huang, P. A. Taylor, K. A. Zaghoul, C. Lungu, *et al.*, "DBSproc: An Open Source Process for DBS Electrode Localization and Tractographic Analysis," *Human Brain Mapping*, vol. 37, pp. 422-433, Jan 2016.
- [83] A. Horn, N. Li, T. A. Dembek, A. Kappel, C. Boulay, S. Ewert, *et al.*, "Lead-DBS v2: Towards a comprehensive pipeline for deep brain stimulation imaging," *Neuroimage*, vol. 184, pp. 293-316, Sep 1 2018.
- [84] E. J. Brunenberg, A. Vilanova, V. Visser-Vandewalle, Y. Temel, L. Ackermans, B. Platel, *et al.*, "Automatic trajectory planning for deep brain stimulation: a feasibility study," *Med Image Comput Comput Assist Interv*, vol. 10, pp. 584-92, 2007.
- [85] R. R. Shamir, I. Tamir, E. Dabool, L. Joskowicz, and Y. Shoshan, "A Method for Planning Safe Trajectories in Image-Guided Keyhole Neurosurgery," *Medical Image Computing and Computer-Assisted Intervention - Miccai 2010, Pt Iii*, vol. 6363, pp. 457+, 2010.
- [86] K. A. Sillay, L. M. Kumbier, C. Ross, M. Brady, A. Alexander, A. Gupta, *et al.*, "Perioperative Brain Shift and Deep Brain Stimulating Electrode Deformation Analysis: Implications for rigid and non-rigid devices," *Annals of Biomedical Engineering*, vol. 41, pp. 293-304, Feb 2013.
- [87] N. Hamze, A. Bilger, C. Duriez, S. Cotin, and C. Essert, "Anticipation of Brain Shift in Deep Brain Stimulation Automatic Planning," *2015 37th Annual International Conference of the Ieee Engineering in Medicine and Biology Society (Embc)*, pp. 3635-3638, 2015.
- [88] M. Bot, P. van den Munckhof, R. Bakay, G. Stebbins, and L. V. Metman, "Accuracy of Intraoperative Computed Tomography during Deep Brain Stimulation Procedures: Comparison with Postoperative Magnetic Resonance Imaging," *Stereotactic and Functional Neurosurgery*, vol. 95, pp. 183-188, Jul 2017.
- [89] Z. Q. Cui, L. S. Pan, H. F. Song, X. Xu, B. N. Xu, X. G. Yu, *et al.*, "Intraoperative MRI for optimizing electrode placement for deep brain stimulation of the subthalamic nucleus in Parkinson disease," *Journal of Neurosurgery*, vol. 124, pp. 62-69, Jan 2016.
- [90] S. A. Ahmadi, F. Milletari, N. Navab, M. Schuberth, A. Plate, and K. Botzel, "3D transcranial ultrasound as a novel intra-operative imaging technique for DBS surgery: a feasibility study," *International Journal of Computer Assisted Radiology and Surgery*, vol. 10, pp. 891-900, Jun 2015.
- [91] U. Walter, "Transcranial sonography-assisted stereotaxy and follow-up of deep brain implants in patients with movement disorders," *Int Rev Neurobiol*, vol. 90, pp. 274-85, 2010.
- [92] M. Luo, S. Narasimhan, A. J. Martin, P. S. Larson, and M. I. Miga, "Model-based correction for brain shift in deep brain stimulation burr hole procedures: a comparison using interventional magnetic resonance imaging," *Medical Imaging 2018: Image-Guided Procedures, Robotic Interventions, and Modeling*, vol. 10576, 2018.
- [93] V. Hesselmann, B. Sorger, R. Girnus, K. Lasek, M. Maarouf, C. Wedekind, *et al.*, "Intraoperative functional MRI as a new approach to monitor deep brain stimulation in Parkinson's disease," *European Radiology*, vol. 14, pp. 686-690, Apr 2004.
- [94] R. Erasmí, O. Granert, D. Zorenkov, D. Falk, F. Wodarg, G. Deuschl, *et al.*, "White Matter Changes Along the Electrode Lead in Patients Treated With Deep Brain Stimulation," *Front Neurol*, vol. 9, p. 983, 2018.
- [95] A. Horn, G. Wenzel, F. Irmen, J. Huebl, N. Li, W. J. Neumann, *et al.*, "Deep brain stimulation induced normalization of the human functional connectome in Parkinson's disease," *Brain*, vol. 142, pp. 3129-3143, Oct 1 2019.
- [96] G. Gilmore, D. H. Lee, A. Parrent, and M. Jog, "The current state of postoperative imaging in the presence of deep brain stimulation electrodes," *Mov Disord*, vol. 32, pp. 833-838, Jun 2017.
- [97] M. C. Keuken, P. L. Bazin, A. Schafer, J. Neumann, R. Turner, and B. U. Forstmann, "Ultra-high 7T MRI of structural age-related changes of the subthalamic nucleus," *J Neurosci*, vol. 33, pp. 4896-900, Mar 13 2013.
- [98] K. Ashkan, P. Blomstedt, L. Zrinzo, S. Tisch, T. Yousry, P. Limousin-Dowsey, *et al.*, "Variability of the subthalamic nucleus: the case for direct MRI guided targeting," *Br J Neurosurg*, vol. 21, pp. 197-200, Apr 2007.
- [99] E. J. Brunenberg, B. Platel, P. A. Hofman, B. M. Ter Haar Romeny, and V. Visser-Vandewalle, "Magnetic resonance imaging techniques for visualization of the subthalamic nucleus," *J Neurosurg*, vol. 115, pp. 971-84, Nov 2011.
- [100] S. A. Eisenstein, J. M. Koller, K. D. Black, M. C. Campbell, H. M. Lugar, M. Ushe, *et al.*, "Functional anatomy of subthalamic nucleus stimulation in Parkinson disease," *Ann Neurol*, vol. 76, pp. 279-95, Aug 2014.
- [101] T. A. Dembek, J. Roediger, A. Horn, P. Reker, C. Oehr, H. S. Dafsari, *et al.*, "Probabilistic sweet spots predict motor outcome for deep brain stimulation in Parkinson disease," *Ann Neurol*, vol. 86, pp. 527-538, Oct 2019.
- [102] J. M. Aveccillas-Chasin and C. R. Honey, "Modulation of Nigrofugal and Pallidofugal Pathways in Deep Brain Stimulation for Parkinson Disease," *Neurosurgery*, Dec 12 2019.
- [103] V. A. Coenen, T. E. Schlaepfer, B. Varkuti, P. R. Schuurman, P. C. Reinacher, J. Voges, *et al.*, "Surgical decision making for deep brain stimulation should not be based on aggregated normative data mining," *Brain Stimul*, vol. 12, pp. 1345-1348, Nov - Dec 2019.
- [104] J. C. Lau, A. R. Khan, T. Y. Zeng, K. W. MacDougall, A. G. Parrent, and T. M. Peters, "Quantification of local geometric distortion in structural magnetic resonance images: Application to ultra-high fields," *Neuroimage*, vol. 168, pp. 141-151, Mar 2018.
- [105] S. Pallavaram, B. M. Dawant, M. S. Remple, J. S. Neimat, C. Kao, P. E. Konrad, *et al.*, "Effect of brain shift on the creation of functional atlases for deep brain stimulation surgery," *Int J Comput Assist Radiol Surg*, vol. 5, pp. 221-8, May 2010.
- [106] Y. Miyagi, F. Shima, and T. Sasaki, "Brain shift: an error factor during implantation of deep brain stimulation electrodes," *Journal of Neurosurgery*, vol. 107, pp. 989-997, Nov 2007.
- [107] Y. Xiao, H. Rivaz, M. Chabanas, M. Fortin, I. Machado, Y. Ou, *et al.*, "Evaluation of MRI to ultrasound registration methods for brain shift correction: The CuRIOUS2018 Challenge," *IEEE Trans Med Imaging*, Aug 13 2019.
- [108] V. M. Saenger, J. Kahan, T. Foltynie, K. Friston, T. Z. Aziz, A. L. Green, *et al.*, "Uncovering the underlying mechanisms and whole-brain dynamics of deep brain stimulation for Parkinson's disease," *Sci Rep*, vol. 7, p. 9882, Aug 29 2017.
- [109] A. Hojlund, M. V. Petersen, K. S. Sridharan, and K. Ostergaard, "Worsening of Verbal Fluency After Deep Brain Stimulation in Parkinson's Disease: A Focused Review," *Comput Struct Biotechnol J*, vol. 15, pp. 68-74, 2017.
- [110] D. Anderson, G. Beecher, and F. Ba, "Deep Brain Stimulation in Parkinson's Disease: New and Emerging Targets for Refractory Motor and Nonmotor Symptoms," *Parkinsons Disease*, 2017.
- [111] A. Stefani, A. Peppe, M. Pierantozzi, S. Galati, V. Moschella, P. Stanzione, *et al.*, "Multi-target strategy for Parkinsonian patients: the role of deep brain stimulation in the centromedian-parafascicular complex," *Brain Res Bull*, vol. 78, pp. 113-8, Feb 16 2009.
- [112] M. V. Petersen, J. Mlakar, S. N. Haber, M. Parent, Y. Smith, P. L. Strick, *et al.*, "Holographic Reconstruction of Axonal Pathways in the Human Brain," *Neuron*, vol. 104, pp. 1056-1064 e3, Dec 18 2019.
- [113] E. Hoppe, G. Korzdorfer, T. Wurfl, J. Wetzl, F. Lugauer, J. Pfeuffer, *et al.*, "Deep Learning for Magnetic Resonance Fingerprinting: A New Approach for Predicting Quantitative Parameter Values from Time Series," *Stud Health Technol Inform*, vol. 243, pp. 202-206, 2017.
- [114] J. V. Manjón, P. Coupé, L. Concha, A. Buades, D. L. Collins, and M. Robles, "Diffusion weighted image denoising using overcomplete local PCA," *PloS one*, vol. 8, pp. e73021-e73021, 2013.
- [115] C. Pham, A. Ducournau, R. Fablet, and F. Rousseau, "Brain MRI super-resolution using deep 3D convolutional networks," in *2017 IEEE 14th International Symposium on Biomedical Imaging (ISBI 2017)*, 2017, pp. 197-200.
- [116] I. Schlesinger, A. Sinai, and M. Zaaroor, "MRI-Guided Focused Ultrasound in Parkinson's Disease: A Review," *Parkinsons Dis*, vol. 2017, p. 8124624, 2017.
- [117] R. B. Kochanski and S. Sani, "Awake versus Asleep Deep Brain Stimulation Surgery: Technical Considerations and Critical Review of the Literature," *Brain Sci*, vol. 8, Jan 19 2018.

Article title: Image guidance in deep brain stimulation surgery to treat Parkinson's disease: a review**Authors: Yiming Xiao, Johnathan C Lau, Dimuthu Hemachandra, Greydon Gilmore, Ali R. Khan, and Terry M. Peters****Table S1.** Specialized MRI sequences for visualizing surgical targets of deep brain stimulation.

Authors	Field strength	No. of subjects	MRI sequence	Anatomical structure	Resolution	Imaging time	Evaluation	Conclusion
Ishmori et al. (2007)	1.5T	3 healthy & 2 patients	3D phase-sensitive inversion recovery	STN	$1 \times 1 \times 2 \text{ mm}^3$	16:56 min	Less than 1% geometric distortion; Measured STN coordinates agree with the landmark-based approach	The sequence offers distortion-free images for DBS targeting
Kitajima et al. (2008)	3T	4 healthy & 20 patients	FSTIR	STN	$0.39 \times 0.625 \times 2.5 \text{ mm}^3$	5:25 min	Contrast ratio between STN and adjacent tissues: 0.10–0.23	FSTIR is superior than T2w FSE in the STN targeting
Sudhyadhom et al. (2009)	3T	3 patients	FGATIR	GPi, STN, Vim	$0.8 \times 0.8 \times 1 \text{ mm}^3$	11:14 min	CNRs of STN, GPi and Vim against surrounding tissues: 5.96, 6.06 & 7.27	FGATIR reveals richer anatomical features than conventional T1w and T2w MRI
Vertinsky et al. (2009)	3T	8 healthy	SWI phase map using SENSE	STN	$0.55 \times 0.75 \times 1.5 \text{ mm}^3$	< 2:30 min	Best visual scores based on 3 raters with TE=20ms and SENSE=1.40	Delineation of the STN was superior in phase images
Volz et al. (2009)	3T	4 healthy & 4 patients	T2*w multi-echo FLASH	STN	$1 \times 1 \times 2 \text{ mm}^3$	3:30 min	Mean CNR of STN vs. WM: 37.1	Combining multi-echo information can reduce susceptibility artifacts and improves the STN contrast
Abosch et al. (2010)	7T	6 healthy	SWI	GPi, STN & Vim	$0.95 \times 0.95 \times 0.95 \text{ mm}^3$	15:00 min	Qualitative visual comparison promotes SWI over T2w MRI in subcortical structure visualization	MRI at 7 T have yielded improved anatomic resolution of deep brain structures

Supplementary material

Cho et al. (2010)	7T	11 healthy & 1 patient	2D GRE (T2*w)	STN, GPi	$0.25 \times 0.25 \times 2 \text{ mm}^3$	5:54 min	Mean normalized intensity difference of STN vs. SN: ~ 0.20 ; only visual assessments for GPi	7T MRI images showed marked improvements in visualization STN and GPi than 3T
Y. Xiao et al. (2012)	3T	4 healthy & 2 patients	Multi-contrast Multi-echo FLASH sequence (R2* & SWI)	STN	$0.95 \times 0.95 \times 0.95 \text{ mm}^3$	7:05 min	Contrast ratio between STN and SN: 0.31 (R2*map) 0.36 (T2*w)	Improved scan efficiency (multiple contrasts in one shot) and STN contrast with lower image distortion
Duchin et al. (2012)	7T	12 patients	TSE	STN	$0.39 \times 0.39 \times 2 \text{ mm}^3$	5:30 min	No contrast assessments	7 T MRI has comparable distortion in central region to 1.5T MRI, and can be used for DBS surgery
Deistung et al. (2013)	7T	9 healthy	Multi-orientation GRE (QSM)	STN, GPi & Vim	$0.4 \times 0.4 \times 0.4 \text{ mm}^3$	16:57 min	Visual assessments for nuclei contrasts	High resolution QSM offers superb contrast for subcortical structures for the STN, GPi & Vim
Nowacki et al. (2015)	3T	13 patients	MDEFT	GPi	$1 \times 1 \times 1 \text{ mm}^3$	12:00 min	MDEFT-based targeting offers 1.07mm error from the actual lead position	Direct targeting of GPi based on MDEFT is accurate and reliable.

Supplementary material

Table S2. Automatic segmentation algorithms for subthalamic nucleus (STN).

Authors	Field strength	No. of Subjects	Image contrasts	Resolution	Algorithm	Dice score
Xiao et al. (2012)	3T	3 healthy & 3 patients	T2w & T2*w	0.95×0.95×0.95 mm ³	Multi-contrast label propagation	L: 0.63±0.06; R: 0.61±0.06
Haegelen, et al. (2013)	3T	10 patients	T1w	1×1×1 mm ³	label propagation (ANIMAL registration)	L: 0.641±0.004; R: 0.640±0.006
Haegelen, et al. (2013)	3T	10 patients	T1w	1×1×1 mm ³	label propagation (SyN registration)	L: 0.626±0.003; R: 0.640±0.006
Haegelen, et al. (2013)	3T	10 patients (leave-one-out)	T2w	1×1×1 mm ³	Nonlocal means patched-based label fusion	L: 0.631±0.005; R: 0.575±0.022
Xiao et al. (2014)	3T	10 patients (leave-one-out)	T2w	1×1×1 mm ³	Fuzzy label-fusion method	L: 0.74±0.08; R: 0.77±0.05
Xiao et al. (2015)	3T	10 patients (leave-one-out)	T2*w & phase	0.95×0.95×0.95 mm ³	Multi-contrast nonlocal means label-fusion method	L: 0.877±0.026; R: 0.900±0.048
Kim et al. (2015)	1.5T & 7T	26 patients (16 training & 10 testing)	T1w & T2w	Not provided	Feature-based shape prediction to transfer knowledge from 7T to 1.5T	L: 0.624±0.002; R: 0.659±0.011
Visser et al. (2016)	3T & 7T	53 healthy	T1w, T2w, T2*w, QSM, FA	0.5×0.5×0.5 mm ³	Multi-contrast intensity-based generative model	~0.8
Park et al. (2019)	3T	102 patients (data augmentation added, 80 for training)	T2*w	0.375×0.375×0.375 mm ³	Deep convolutional neural network	0.902
Manjon et al. (2020)	3T	15 healthy (leave-two-out)	T2w	0.5×0.5×0.5 mm ³	Multi-atlas patch-based label fusion with multi-scales and multi-features	L:0.856; R: 0.855

Supplementary material

Table S3. Survey of functional targeting methods for deep brain stimulation in treating Parkinson's disease (sMRI=structural MRI, DWI=diffusion-weighted imaging, fMRI= functional MRI).

Author & Year	Target	Method	No. of subjects	Data modality	Reference space	Outcomes	Ground truth
Guo et al. (2005)	STN	Construct a functional atlas that contain electrophysiological data	131 patients for atlas construction & 8 patients for testing	sMRI, physiological recording	CJH-27 atlas	2.84 mm (Absolute differences between the centroids of the segmented STN and the real targets)	Real target location
D'Haese et al. (2005)	STN	Automatic selection of DBS target points using multiple electrophysiological atlases	14 patients	sMRI and electrophysiological recording	Schaltenbrand-Wharen atlas	Mean deviation from final implant: 1.66 mm (Left) and 1.74 mm (right)	final implantation position in post-op CT
Nowinski et al. (2007)	STN	Construct a probabilistic functional atlas that represents spatial frequency of best contacts	184 patients	sMRI, Physiological recordings	AC-PC based cartesian space	The "hot" functional STN resides inside anatomical STN	Coordinates in Schaltenbrand-Wahren atlas
Sammartino et al. (2016)	Vim	Tractography-based methodology for the stereotactic targeting of the ventral intermediate nucleus	14 patients and 15 healthy subjects	DWI	subject native space	Euclidean distance between tractography-based and surgical target was 1.6+/- 1.1mm	Intra-operative stimulation & landmark-based targeting
Pallavaram et al. (2008)	STN	A probabilistic efficacy map was constructed with a spherical shell kernel	19 patients (95 stimulation data)	T1w MRI, and clinical assessments	In-house atlas space	Final stimulation locations are within the "hot zones" of the efficacy map	final implantation position in post-op CT
Anderson et al. (2011)	Vim	A finger movement task is used to trigger activation in relevant regions	58 healthy subjects	fMRI	MNI space	Within 3 mm of clinically optimized targets	Optimized targets based on anatomical landmarks
Horn et al. (2017)	STN	Linear regression based on functional and structural connectomic patterns is used to predict motor symptom improvements	51 patients for training and 44 patients for testing	fMRI & DWI	MNI space	An average error of 15% UPDRS improvement	Post-surgical UPDRS motor scores

Supplementary material

Akam et al. (2017)	STN	Voxel-based statistical analysis was used to identify significant treatment clusters, which was mapped to relevant cortical regions	20 patients	T1w MRI & DWI	MNI space	The maximum overall efficacy is X=-10(-9.5) mm, Y=-13(-1) mm and Z=-7(-3) mm in MNI(AC-PC) space.	functional outcomes before and 1-yr after surgery
Baumgarten et al. (2018)	STN	An artificial neural network is trained based on stimulation loci coordinates and electric current to predict therapeutic benefits and side effects	30 patients (130 tested electrode positions)	T1w MRI and clinical assessments	ParkMedAtlas atlas	The mean sensitivity and specificity were 93.07% and 69.24% for the therapeutic effect, 73.47% and 91.82% for the side effect	Therapeutic and side effects (no effect, partial effect, or full effect) 3 months before and after surgery
Middlebrooks et al. (2018)	GPi	10 segments of GPi is derived from structural connectivity to 10 cortical and subcortical structures; activation of each segment is correlated with motor symptom improvements	11 patients	T1w MRI & DWI	Subject native space	GPi segments related to primary and supplementary motor areas are strongly correlated with UPDRSIII improvement	UPDRSIII scores from preoperative and 6-month follow-up visits
Coenen et al, (2020)	DRT	DRT was tracked and used as a direct thalamic or subthalamic target	36 patients	T1w & T2w MRI, DWI	Subject native space	Close distance to the DRT is correlated with tremor reduction	Surgical outcomes
Lin et al. (2020)	STN	Random forest classifier based on mean FA and streamline fraction	58 patients for training, 19 for testing	T1w & T2w MRI, DWI	Subject native space	84.9% accuracy to discriminate ineffective targets	Surgical outcomes

Supplementary material

Table S4. Public surgical navigation software for deep brain stimulation (sMRI=structural MRI, DWI=diffusion-weighted imaging).

Name	Platform	Imaging modality	Trajectory planning	Electrode reconstruction	targeting technique	Preinstalled atlas
CranialVault (D'Haese et al., 2012)	CRAVE	CT & sMRI	Yes	Yes	Based on probabilistic functional atlas	In-house electrophysiological and subcortical atlases
PyDBS (D'Albis et al., 2015)	3D Slicer	sMRI	yes	No	Based on structural atlas	In-house population-averaged 3T MRI atlases (T1w & sectional T2w) of PD patients
DBSproc (Lauro et al., 2016)	AFNI	sMRI, DWI & CT	No	Yes	Patient-specific direct targeting	N/A
IBIS (Drouin et al., 2017)	IBIS neuronav	sMRI, angiography, CT	Yes	No	Based on structural atlas	N/A
Lead-DBS (Horn et al., 2018)	MATLAB	sMRI, tracrography	No	Yes	Based on structural and connectomic atlases	17 cortical & 18 subcortical public atlases and averaged brain connectomic atlas
PaCER (Husch et al., 2018)	MATLAB	sMRI & CT	No	Yes	NA	N/A